Transaction A: Civil Engineering
Vol. 16, No. 5, pp. 376–387

SCIENTIA IRANICA

A Numerical Study on the Effect of Accident Configuration on Pedestrian Lower Extremity Injuries

S. Shahbeyk[1,*] and A. Abvabi[2]

Abstract. *An FE model of a pedestrian lower legform impactor has been developed and certified, both statically and dynamically, based on EEVC-WG17 requirements. The legform is then utilized in a series of 40 km/hr pedestrian accident analyses to assess the protection level delivered by a typical sedan vehicle. The values of maximum tibia acceleration, maximum knee bending angle, and maximum knee shearing displacement have been extracted for 25 different accident configurations and compared with their admissible ranges. It has been shown that tibia acceleration is mainly influenced by extension of the area transferring the impact load between the legform and the vehicle. However, variations of vehicle front-end structure geometry and stiffness in the vertical direction have been found to be the most decisive parameters in the level of legform knee maximum bending rotation and maximum shearing displacement.*

Keywords: *Pedestrian accident; Lower extremity injury; Bumper design.*

INTRODUCTION

Based on the statistics reported by International Harmonized Research Activities (IRHA), pedestrian accidents annually take a toll of 20,000 lives in North America, EU, Korea and Japan [1]. Adding half a million individuals seriously injured to the casualties, one can clearly understand how tragic the consequences are. Since injuries to pedestrians are likely to take a long time to rehabilitate and cause lots of permanent disabilities, growing efforts are being made around the world to design more pedestrian-friendly vehicles. The approaches utilized in this research can be categorized as experimental, multi-body dynamics, FE modeling, or a combination of all. In [2,3], the head injury level experienced by a pedestrian when he or she collides with a vehicle hood has been studied using full scale experimentally certified MADYMO multi-body models. The main influencing parameters have been identified as being local stiff points inside the hood structure, geometrical features, such as ribs, proximity to the hard engine parts just beneath the impact points, and head traveling velocity. In [4,5], the same method has been applied for the optimization of vehicle front-end structures. The method is further used in the assessment of head injury criterion for head-road surface collisions [6]. In other studies, full scale or subsystem finite element based simulations are used to estimate the pedestrian head injury level [7,8]. Replacing steel structures with softer aluminum based assemblies has been the subject of some studies to reduce the aggressiveness of vehicle hoods against the heads of adults and children [9-11].

Leg injuries, with a share of around 40%, have the biggest frequency in nonfatal pedestrian accidents. Similar to the problem of head protection in pedestrian accidents, many studies have been accomplished using experimental, multi-body dynamics, and full scale FE modeling approaches to identify the decisive parameters affecting the level of leg injuries [12-15]. The most important outcomes of such research can be identified visually when someone gives attention to the geometrical design of bumpers in newly introduced vehicles.

In a parallel effort to the afore-mentioned independent studies, unified activities have been carried out in recent years to establish a harmonized method of safety assessment in pedestrian accidents. The results

1. *Department of Civil Engineering, Tarbiat Modares University, Tehran, P.O. Box 14115-143, Iran.*
2. *CAE Department, Iran Khodro (IKCo) Research and Development Center, km 14 Karaj Road, Tehran, P.O. Box 13895-111, Iran.*
*. *Corresponding author. E-mail: shahbeyk@modares.ac.ir*

Received 1 June 2008; received in revised form 5 January 2009; accepted 7 March 2009

of these endeavors led to the development of new test procedures, such as those proposed by the European Enhanced Vehicle Safety Working Group 17 (EEVC-WG17) [16] and the Japanese New Car Assessment Program (JNCAP) [17]. Although none of these regulations are mandatory, they will be put into effect in most developed countries in 2010 [18].

Among all approaches, the way EEVC evaluates pedestrian injuries is one of the most efficient and repeatable routines. The whole procedure contains three subsystems, namely headform, upper-legform and lower-legform, targeting specifically to check the injuries induced by vehicle front structures to the head, pelvic area and lower extremities, respectively [16]. The accuracy of such replacements has been studied through a comparison between EEVC-WG17 recommended subsystems and full scale dummies [19]. Promising agreement is observed for vehicles with low bumper height. In [20-22], an optimized bumper assembly has been constructed using statistical and analytical techniques, respectively. In addition, studies such as [23] can be found in the literature, in which an optimized solution for the contradicting issues of pedestrian safety and the low-speed accident performance of vehicles has been sought.

In the present study, first of all, a lower legform impactor FE model has been developed and certified statically and dynamically based on the specifications and requirements of EEVC-WG17. Then, the model is incorporated in a series of pedestrian accident simulations where the impactor collides with a typical vehicle front-end at a traveling velocity of 40 km/hr. The effects of bumper height and legform lateral eccentricity on maximum knee shearing displacement, maximum knee bending rotation, and maximum tibia acceleration have been investigated.

LOWER LEGFORM FE MODEL

Lower Legform Physical Components

As shown in Figure 1, an EEVC lower legform impactor consists of two metal tubes (representing tibia and femur) with an outer diameter of 70 ± 1 mm, 25 mm thick CF45 Confor^{TM} foam flesh, 5 mm Neoprene skin cover, faced with 0.5 mm thick nylon cloth on both sides; a hinge representing the actual knee joint and a limiting damper attached to the shear system [16]. The total mass and moment of inertia of the femur and tibia shall be 8.6 ± 0.1 kg, 0.127 ± 0.010 kgm^2, and 4.8 ± 0.1 kg, 0.120 ± 0.010 kgm^2, respectively. The moment of inertia for each part is defined about a horizontal axis through their center of gravity and perpendicular to the direction of impact. The C.G. of the femur and tibia are 217 ± 10 mm and 233 ± 10 mm away from the center of the knee joint, respectively.

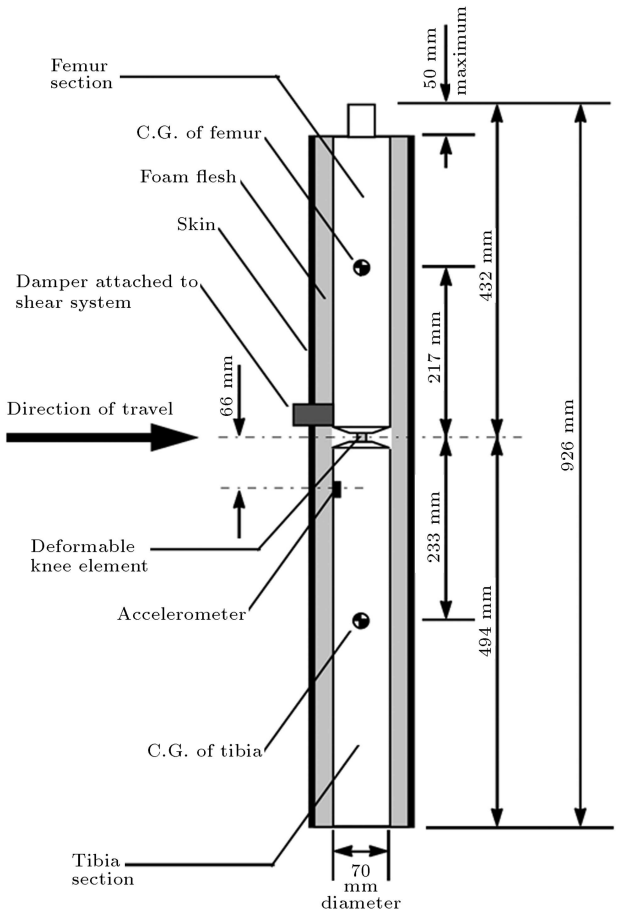

Figure 1. EEVC legform impactor with skin and foam covering [16].

Knee Joint Static Specifications

The behavior of the lower legform in an actual vehicle impact test relies mainly on the shear and bending characteristics of the knee joint. This is why EEVC-WG17 accurately defines the acceptable ranges for shear force-deformation and bending moment-rotation responses of the knee itself through two static tests.

Figures 2 and 3 show the configurations used in the static shear and bending certification tests, respectively. Only metal tubes representing femur and

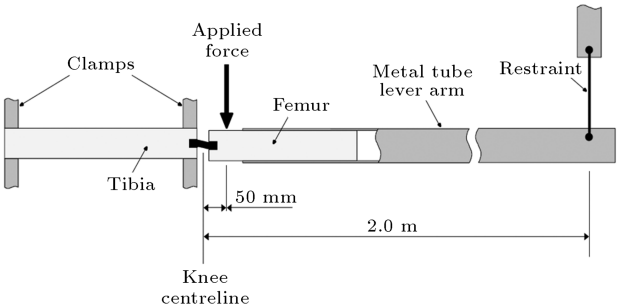

Figure 2. Test set-up for the static legform impactor shearing certification test [16].

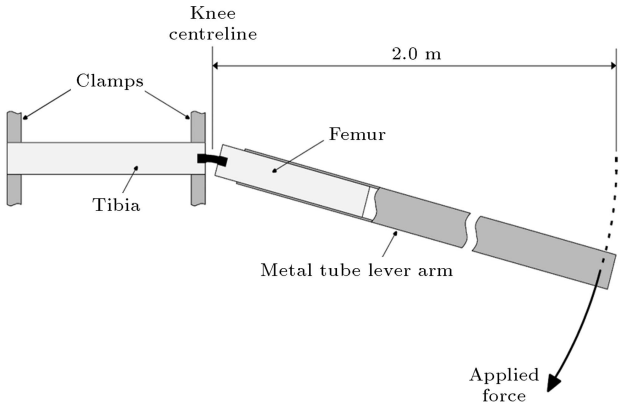

Figure 3. Test set-up for the static legform impactor bending certification test [16].

tibia bones, the knee joint and a metal tube lever arm shall be considered. Clamps are utilized on both sides of the tibia to ensure absolute measurement of knee joint shear deformation or bending rotation. The load application point in the bending test is located 2 m from the knee. The force gradually increases, while its direction remains perpendicular to the tube throughout the loading process. In contrary to the bending test, a point 2 m from the knee is restrained for the static shear test while the shearing force is applied 50 mm away from the knee joint. The measured forces will be plotted against the sharing displacement/bending rotation. Then, these curves shall be compared with the admissible ranges depicted in Figures 4 and 5.

Legform Dynamic Certification Test

In addition to the static tests developed to certify the shear and bending responses of the legform knee joint, a dynamic test on a complete impactor (flesh

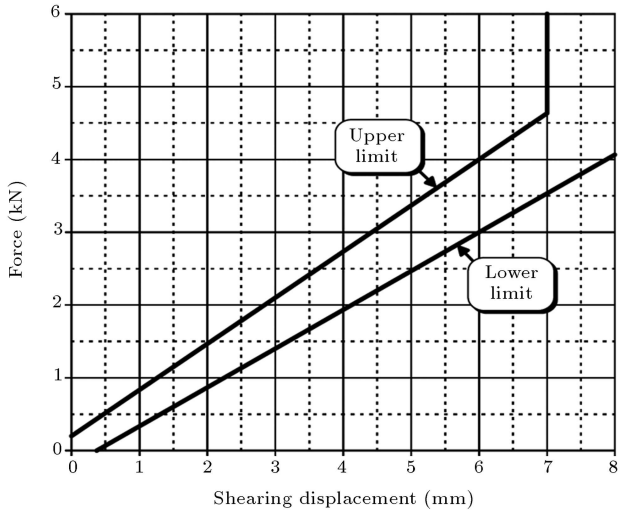

Figure 4. Force versus displacement requirement in static legform impactor shearing certification test [16].

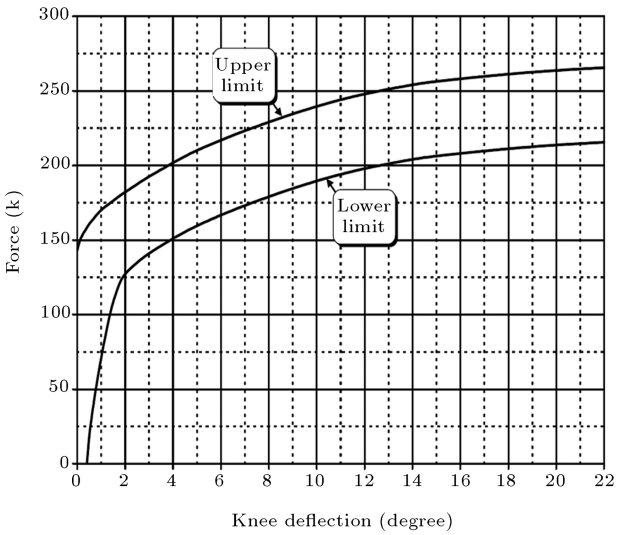

Figure 5. Force versus angle requirement in static legform impactor bending certification test [16].

foam and skin are included) has been designed to ensure the validity of the whole system. Figure 6 presents the configuration of the dynamic test, where a 9.5 kg aluminum impactor specified by EEVC-WG17 approaches at a velocity of 7.0 m/sec to a legform suspended horizontally by 3 steel cables of 2 m height and 2 mm diameter. The impactor moves in the direction perpendicular to the legform longitudinal axis with an eccentricity of 50 mm.

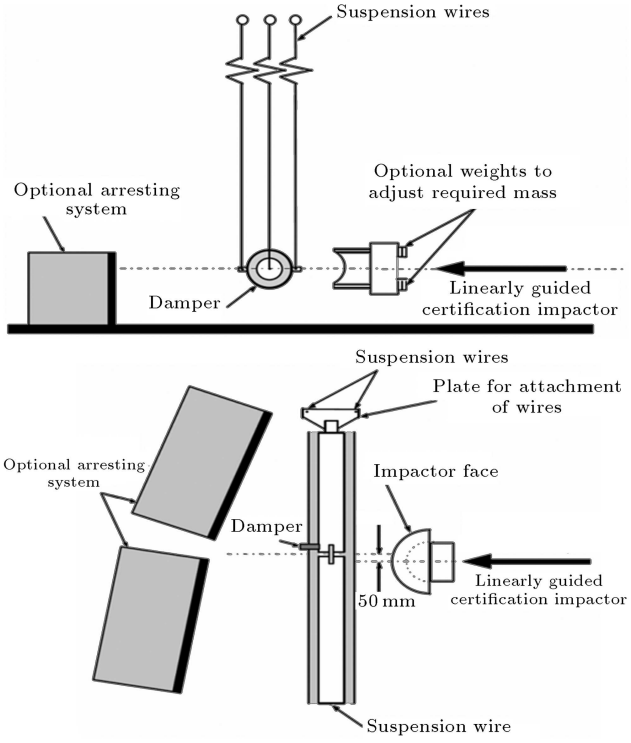

Figure 6. Test set-up for the dynamic legform impactor certification test [16].

Three parameters, namely maximum upper tibia acceleration, maximum knee bending angle and maximum knee shear displacement will be measured and compared to the allowable ranges of 120-250 g, 6.2-8.2 degrees and 3.5-6.0 mm, respectively. The upper tibia acceleration shall be measured at a point 66 mm below the knee joint in the opposite direction to impact.

FE Mesh Preparation

The geometrical modeling of the legform has been done using MSC.PATRAN and PAM-GENERIS preprocessing programs. The metal tubes representing the femur and tibia are considered to react as rigid parts. Hence, only their external surfaces are meshed in shell elements. By applying the density of steel to shells and calculating their weight, in addition to their corresponding flesh and skin shares, the weight and moment of inertia of the femur and tibia have been calculated in the model as being 2.6 kg, 0.0409 kg.m^2 and 2.8 kg, 0.0644 kg.m^2, respectively. As these calculated masses and inertias differ from those required by regulation, lumped masses and inertias have been added to the model, based on the following procedure:

- Two nodal masses of 6.0 and 2.0 kg are added to the femur and tibia, respectively. The locations of these masses are calculated in such a way that the center of gravity of each part coincides with the position required by regulation.
- Two nodal moments of inertia have been added to the C.G. of the femur and tibia ($I = 0.08611$ kg.m^2 for femur and $I = 0.0556$ kg.m^2 for tibia).

Two nodes with similar spatial coordinates are defined in the position of the knee joint. Selecting one of these nodes, a nodal rigid body is defined to connect this node to the C.G., the added nodal mass, and the external surface of the metal tube corresponding to the femur. The other node is used in a similar manner for the tibia assembly.

A discrete beam element has been created between the previously defined nodes to capture the nonlinear rotational and linear translational deformation characteristics of the knee joint, as required by the static tests. In addition, a damper element is added to prevent any probable minor vibrations under actual dynamic loading conditions.

The skin and flesh of the legform are modeled using 8 node hexahedron elements with a reduced integration procedure. The mesh size decreases in the region of severe impact to improve the accuracy of the results. The number of elements corresponding to each type and the minimum and maximum element lengths of the legform components are gathered in Table 1. Figure 7 shows the completed FE model with its individual components.

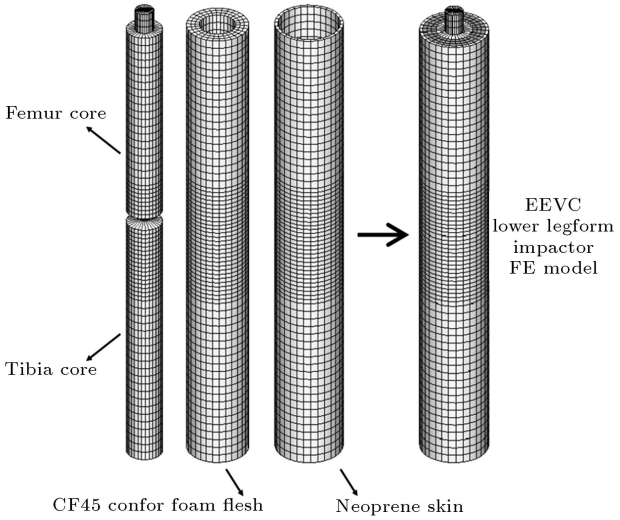

Figure 7. EEVC lower legform impactor FE model.

Material Properties

PAM-CRASH material type 21 (elastic foam with hysteresis for solid elements) is incorporated to model the mechanical response of CF45 Confor^{TM} Foam [24]. The foam uniaxial compressive stress-strain curve is shown in Figure 8. It is used as a base response upon which unloading and hysteretic behavior will be defined. The tensile behavior in the model is assumed to be linear elastic.

PAM-CRASH material type 5 with linear viscoelastic assumption for the deviatoric stress tensor has been applied to the Neoprene skin in which:

$$s_{ij} = \int_0^t (G_\infty + (G_0 - G_\infty)e^{-\beta(t-\tau)}) \frac{\partial \epsilon'_{ij}}{\partial \tau}\, d\tau.$$

G_0 and G_∞ are short-time and long-time shear modules, respectively. Table 2 presents the input data for

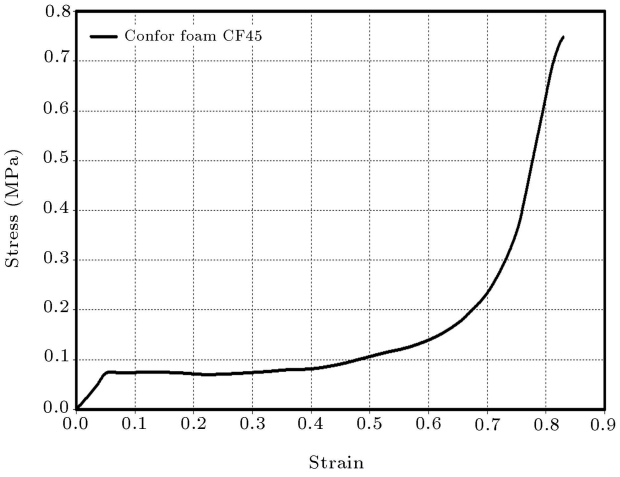

Figure 8. Confor foam CF45 uniaxial compressive stress-strain curve [24].

Table 1. FE meshing data for the lower legform impactor model.

Component	Element Type	Number of Elements	Minimum Element Length (mm)	Maximum Element Length (mm)
Femur	4 node shell	1052	2.34	15.9
Tibia	4 node shell	1232	2.34	15.9
Knee Joint	Discrete beam	1	0	0
Flesh	8 node hexahedral	6209	7.31	15.9
Skin	8 node hexahedral	2069	8.71	15.9

Table 2. Materials input parameters for the legform flesh and skin.

CF45 Confor™ Foam Flesh (PAM-CRASH Material Type 21)		**Neoprene Rubber Skin (PAM-CRASH Material Type 5)**	
Young's modulus	100 MPa	Elastic bulk modulus	102 MPa
Hysteretic unloading factor	0.95	Short time shear modulus	8.45 MPa
Decay constant	100 S^{-1}	Long time shear modulus	3.90 MPa
Viscous coefficient	0.01	Decay constant	500 S^{-1}
Shape factor for unloading	1.0		

both CF45 Confor™ Foam flesh and Neoprene skin, as required by their corresponding models [25].

LEGFORM FE MODEL VALIDATION

Both static and dynamic test procedures outlined in the EEVC-WG17 have been utilized for the final validation of the legform FE model. The analyses have been conducted using PAM-CRASH 2002 explicit finite element code. Figures 9 and 10 present applied force-knee shearing displacement and applied force-knee rotation curves of the legform in sheer and bending static tests, respectively. It is observed that both curves fit appropriately within the ranges addressed by regulation. In addition, the energy taken by the legform FE model in order to generate 15 degrees of the bending angle is 98.9 J compared to the acceptable range of 100 ± 7 J.

An aluminum impactor FE model of 9.5 kg created in MSC.PATRAN environment has been used for the dynamic certification test of the legform (Figure 11). Figures 12-14 show the time histories of the upper tibia acceleration, knee bending angle, and knee shearing displacement, respectively. It is seen that the maximum values of measured parameters fall inside their admissible ranges.

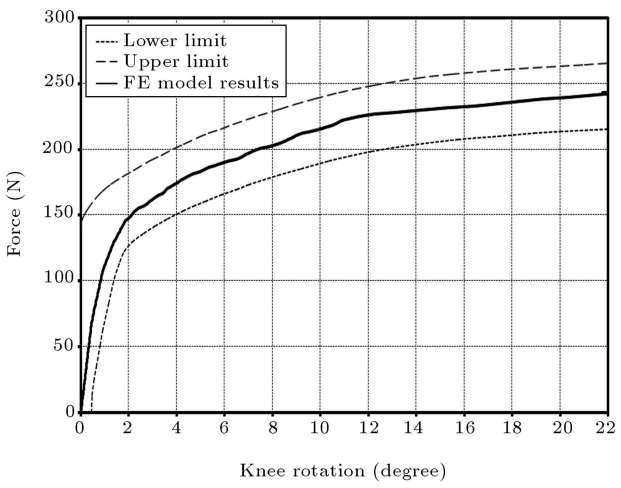

Figure 9. Legform FE model force versus knee bending angle response (EEVC static bending certification test).

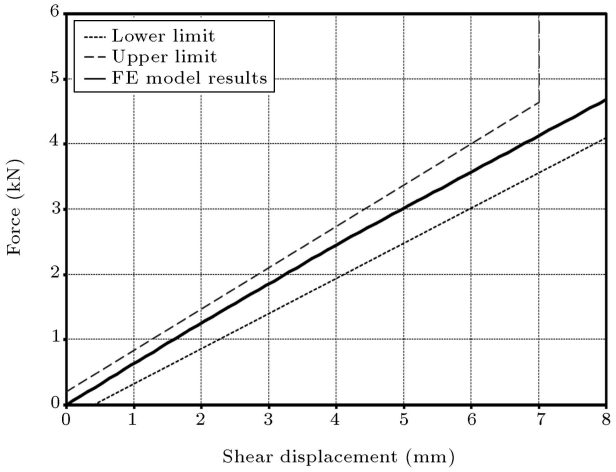

Figure 10. Legform impactor FE model force versus knee shearing displacement response (EEVC static shearing certification test).

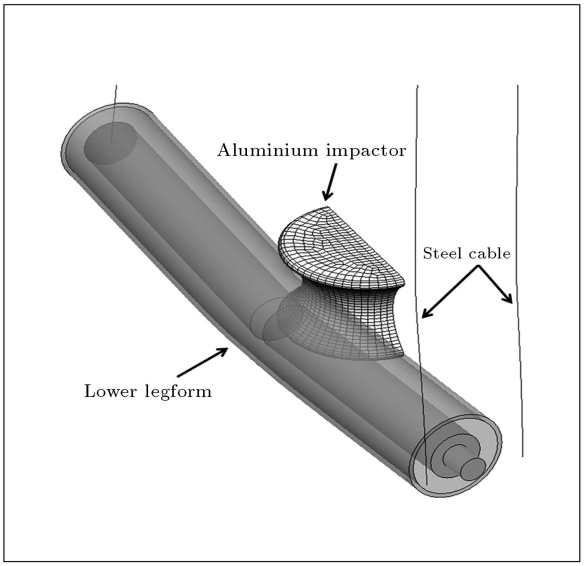

Figure 11. Schematic response of the legform impactor FE model in EEVC dynamic certification test.

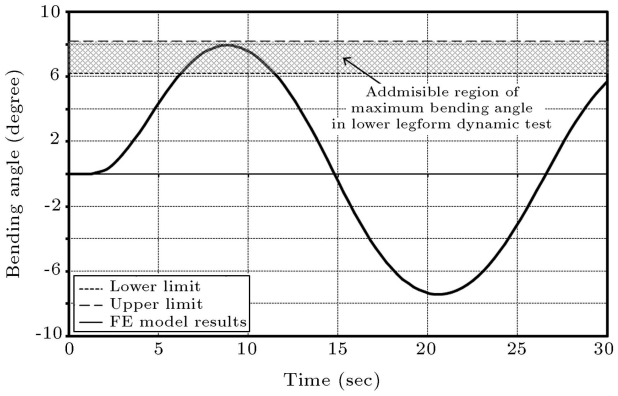

Figure 12. Knee bending angle time history in EEVC dynamic certification test.

VEHICLE - LEGFORM CRASH SIMULATION

A typical vehicle front-end structure, consisting of bumper, shock absorbers, outer fenders, hood assembly and lamps, has been selected and modeled using MSC.PATRAN and PAM-GENERIS (Figure 15). Materials input data corresponding to various components of vehicle front-end structures have been presented in Table 3.

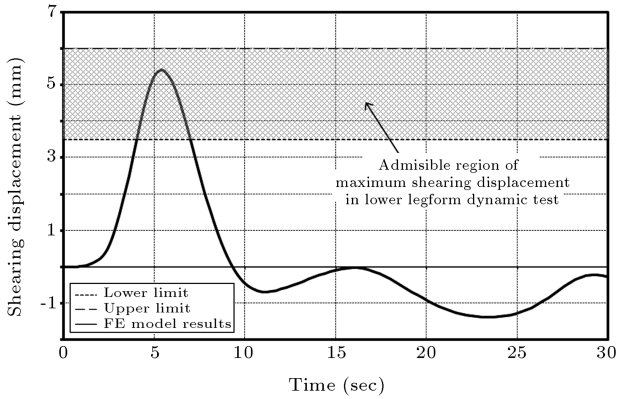

Figure 13. Knee shearing displacement time history in EEVC dynamic certification test.

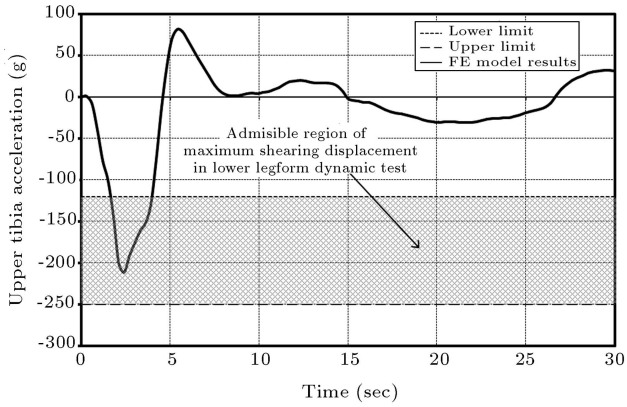

Figure 14. Upper tibia acceleration time history in EEVC dynamic certification test.

The vehicle-legform collisions have been simulated using PAM-CRASH 2002 explicit finite element code. The vehicle front-end structure has been fixed via the definition of a rigid body connecting the supporting points to the C.G. of the vehicle. As illustrated in Figure 16, 25 positioning configurations, consisting of 5 different legform knee heights and 5 different lateral impact point eccentricities, have been adopted for the analyses. An initial velocity of 40 km/h is applied to

Table 3. Materials input parameters for the vehicle front-end components.

Component	Material Type	Density (kg/m^3)	Elastic Modulus (GPa)	Yield Stress (MPa)	Poisson's Ratio
Bumper Skin	Hifax 238	900	1.145	24.5	0.37
Bumper Beam	GMT	1240	5.6	90	0.36
Shock Absorber	P/E	900	1.34	27	0.39
Bumper Fascia	Hifax 238 G9	900	0.9	17	0.37
Hood and Fenders	Steel	7890	210	230	0.30

Figure 15. Vehicle front-end FE model.

the lower legform while the whole model is under the influence of gravity.

RESULTS AND DISCUSSIONS

Figure 17 presents how the developed pedestrian lower legform impactor interacts with a vehicle front-end for a typical 40 km/h collision. Figures 18-20 show the maximum tibia accelerations, maximum knee bending rotations and maximum knee shearing displacements experienced by the lower legform impactor for the 25 different positioning configurations described above, respectively.

From the tibia maximum acceleration point of view, almost all configurations fail to comply with the limiting criterion of 150 g mentioned in EEVC-WG17. As vehicle front-end stiffness is the main influencing parameter on tibia acceleration, if one seeks to pass this requirement, a redesign of the assembly is inevitable.

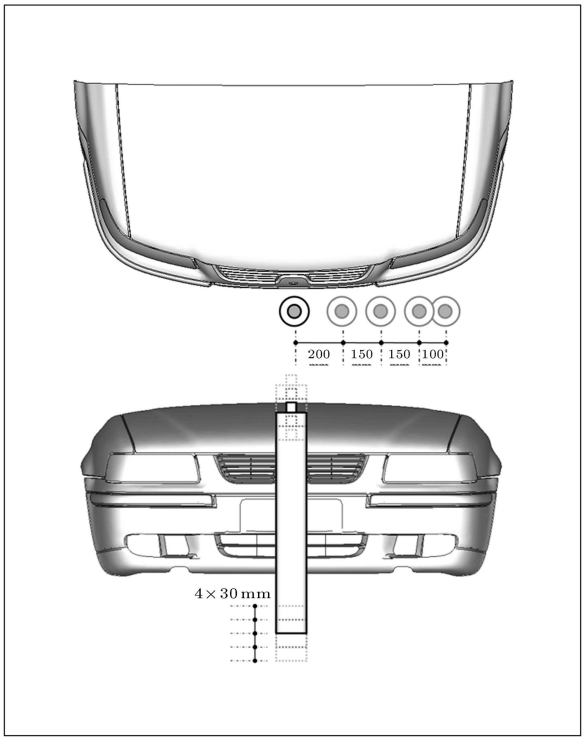

Figure 16. The definition of the legform impactor selected positions in respect to the vehicle front-end structure.

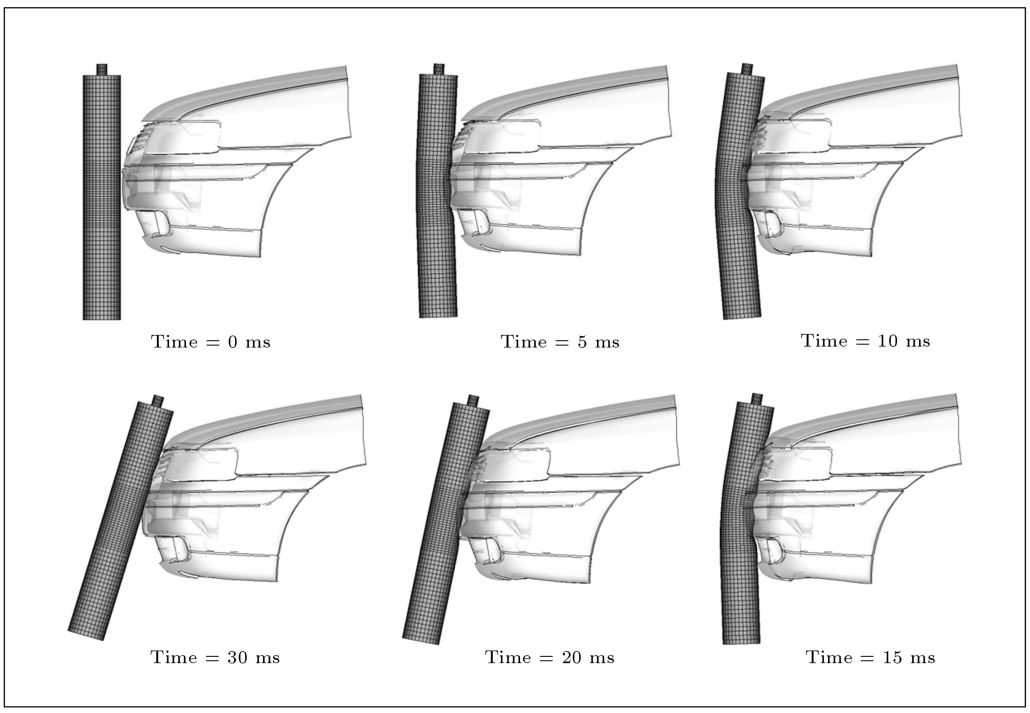

Figure 17. A typical impactor-vehicle interaction in an EEVC lower legform test (LE = 0 mm, LBH = 405 mm).

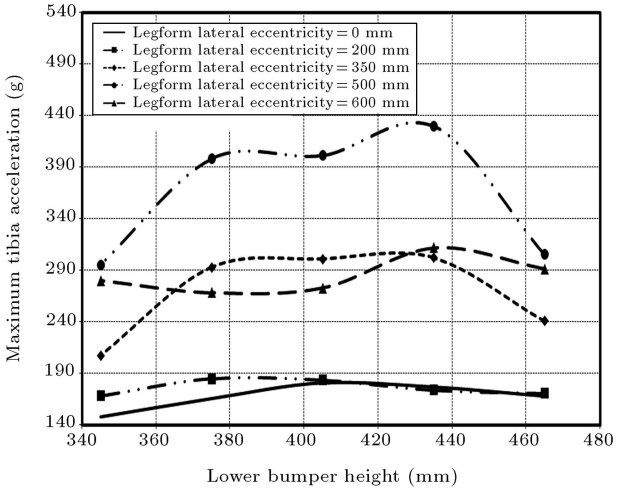

Figure 18. Comparison of the maximum tibia accelerations for different impact positions.

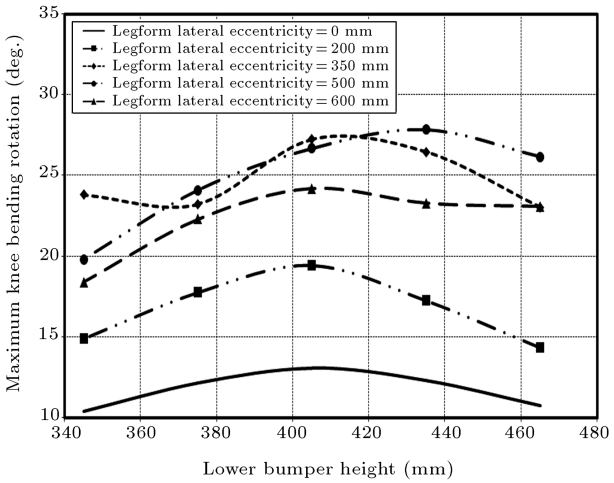

Figure 19. Comparison of the maximum knee bending angles for different impact positions.

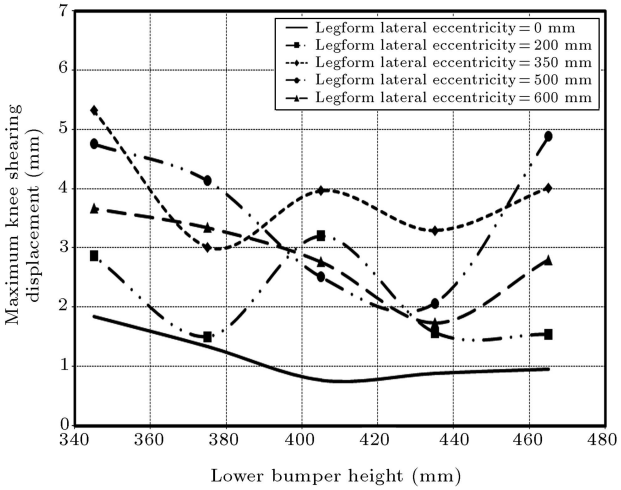

Figure 20. Comparison of the maximum knee shearing displacements for different impact positions.

This can be verified by the results obtained for the configurations with 0 mm and 500 mm eccentricities (Figure 21). In the first case, the bumper beam is impacted in the middle of its supported length where the minimum stiffness is in the direction of impact. It results in a gradual decrease of legform velocity and, therefore, in a lower maximum tibia acceleration. In addition, because the bumper cover is nearly flat in the middle of the vehicle width, no stiffness augmentation is imaginable through the arching action of the shell. However, for a case with 500 mm eccentricity due to the combination of a more concentrated contact area and the presence of a stiff crash box supporting the bumper beam (Figure 21), accelerations as high as 400 g are experienced. In an attempt to reduce this high level of acceleration, the yield stress of the bumper impact beam has been reduced to 20 MPa. Figure 22 compares the distribution of deformations in the original and the modified assembly, where the maximum tibia acceleration has been decreased to less than 200 g. It is worth mentioning that such decisions regarding materials properties and shape of components should be made according to a design strategy package including pedestrian safety, low speed impact, styling and repairability concerns.

In contrast to tibia acceleration, the maximum knee shearing displacements obtained in all analyses are less than the limiting value of 6 mm. As shearing displacement is controlled with the relative longitudinal translocation of tibia and femur, any symmetrical deformation patterns about the knee will give a low value of this parameter. In Figure 23, the sections of

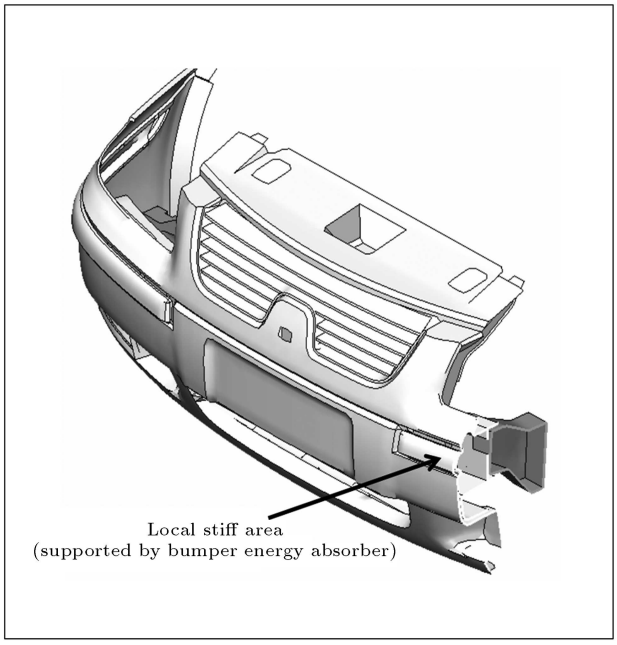

Figure 21. Highly stiff area in the bumper assembly.

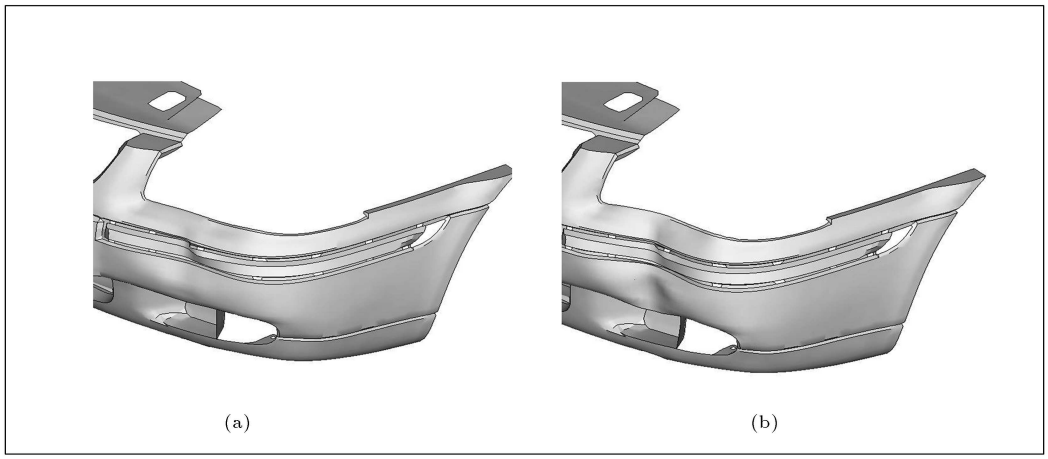

Figure 22. The pattern of deformation on the external surface of the bumper assembly. (a) With original bumper beam; (b) With weakened bumper beam.

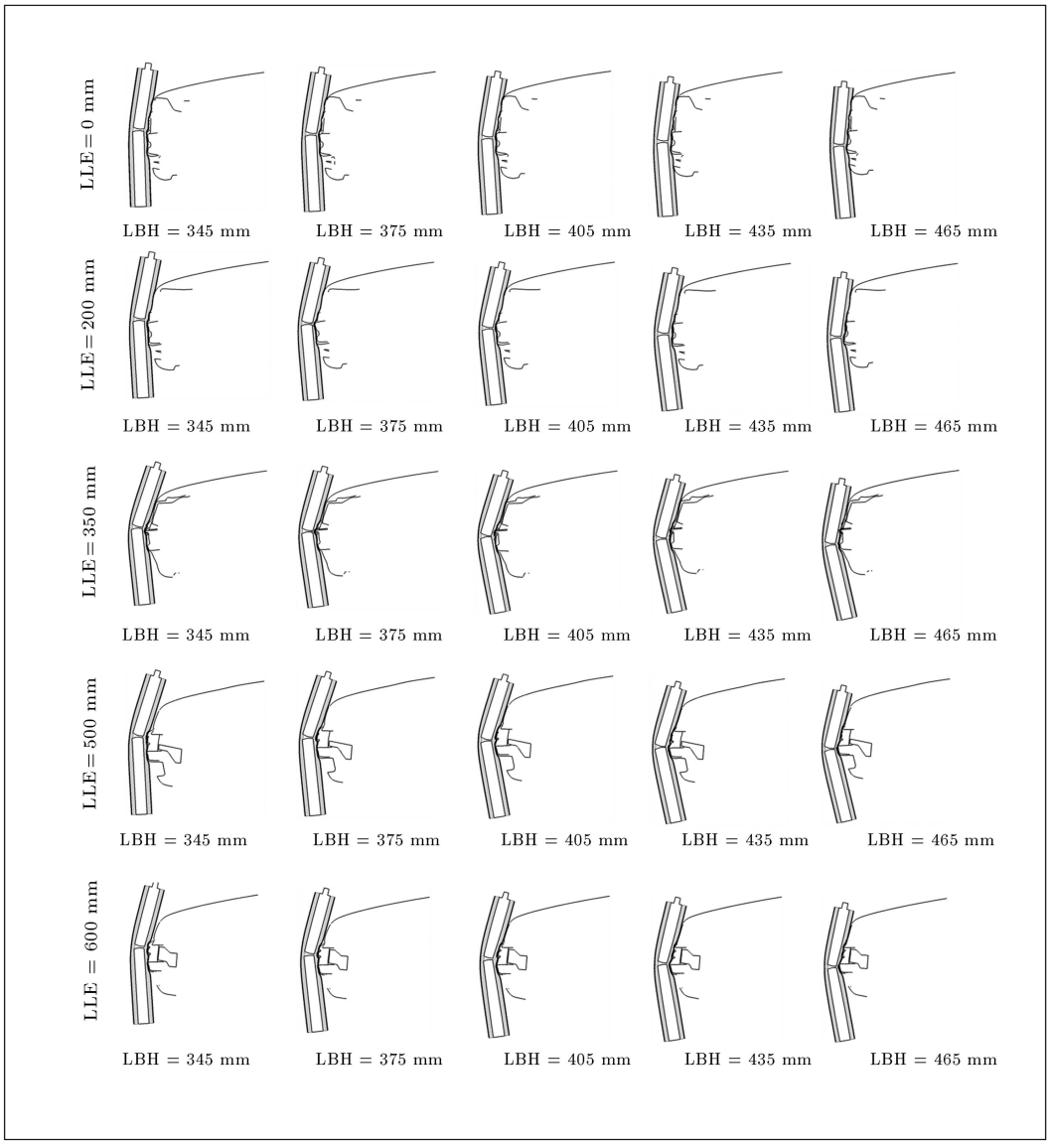

Figure 23. The sections of lower legform impactor at maximum bending rotation for different impact positions.

legform and vehicle front-end are shown for all cases in their maximum deformed shapes. It is seen that symmetry is preserved for most cases with moderate lower bumper heights. However, distancing from the mean LBH (405 mm), symmetrical configuration is disturbed and the knee shearing displacements are accentuated for cases with LBH = 345 mm and LBH = 465 mm.

In some configurations, where the contact force acts well below the knee, a lash like movement is observed as the legform departs the bumper (Figure 24). Such a kinematic pattern alters the symmetrical configuration of the legform and may cause big shearing displacement in the final stages of collision.

When it comes to knee bending rotation, the resisting geometry of the vehicle front-end structure is decisive, i.e. if a uniform crumpling pattern is provided by the vehicle, the legform will experience the least knee rotation possible. This condition has been observed for cases where minimum impactor lateral eccentricity exists (Figures 23 and 25). It is why the middle lateral position satisfies the limiting rotation of 15 degrees for all LBH values (Figure 19). As the legform lateral eccentricity grows, the presence of a more localized resisting structure allows the femur and tibia to rotate freely about the knee joint and results in bending rotations as big as 25 degrees. Because no physically applicable passive solution can be applied to prevent the free motion of the femur (due to styling restrictions), outward stretching of the bumper lower part is the recommended main remedy for reduction of knee rotation. As an example, in order to check the effectiveness of such a modification, a new model has been created in which an elastically supported plate

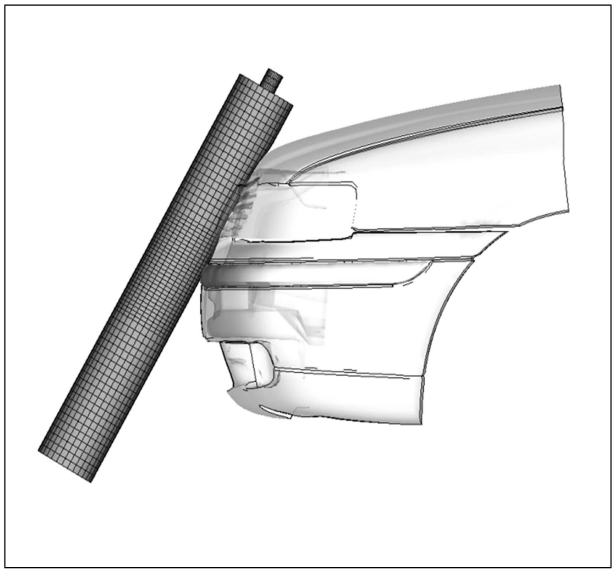

Figure 24. The effect of low contact force location on the legform final configuration (time = 30 ms).

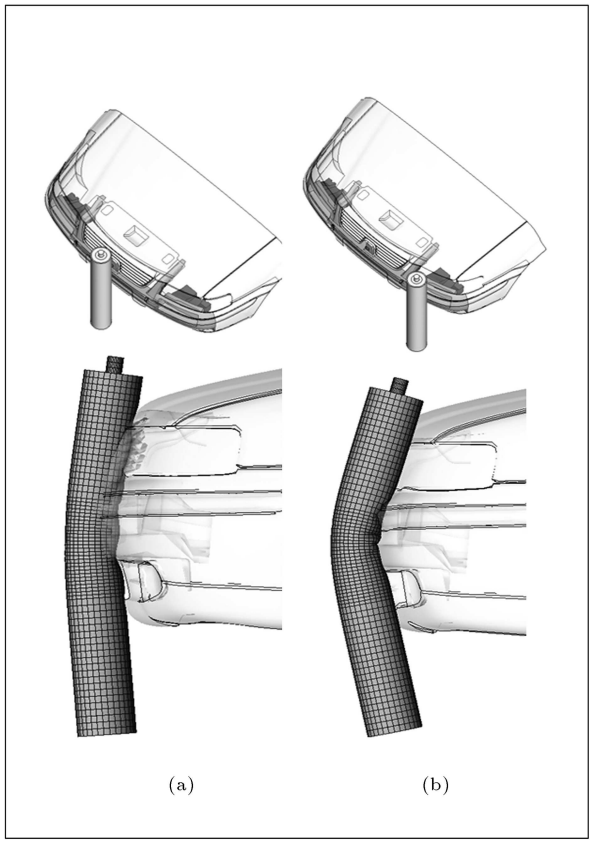

Figure 25. The effect of local stiffness on bending configuration of legform. (a) Collision with the soft part of the bumper assembly; (b) Collision with the stiff part of the bumper assembly.

prevents the lower part of the legform to be overridden. The legform in its maximum bending configuration has been shown in Figure 26 for this new model. A maximum knee bending rotation of 11 degrees has been obtained, which is considerably less than the 27 degrees calculated in the original model.

CONCLUSIONS

A pedestrian lower legform impactor FE model has been developed and certified, both statically and dynamically, based on EEVC-WG17 requirements. Considerable attention is given to the property of the constructive materials and the knee joint response in order to achieve reliable results. In the next stage, the model is used for the lower extremity injury assessment of a typical vehicle front-end structure in the event of pedestrian collision. Five lateral eccentricities, measured from the middle of the vehicle width, and five different lower bumper heights are considered to investigate the effect of impact location and consequently the effect of vehicle front-end geometry and stiffness on legform injury criteria. The maximum tibia acceleration shows a direct connectivity to the local

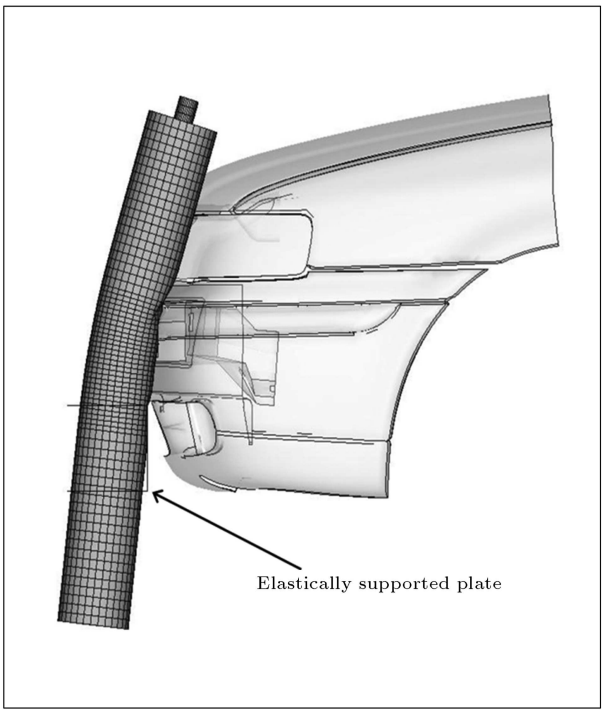

Figure 26. The effect of preventing elastically supported plate on the maximum knee bending angle.

stiffness of the impacting structure near the measuring point. Values ranging from 150 g to 430 g have been recorded as the legform lateral eccentricity changes from zero (when the contacting structure is extremely soft) to its maximum value (stiffer corner assembly). However, for maximum knee shearing displacement and knee maximum bending rotation, the vertical stiffness distribution of the vehicle front-end is found to be decisive.

REFERENCES

1. Chon, D., Uikey, D. and Mohammed, R. "Energy absorber developments and correlation for lower leg pedestrian impact", *SAE 2007-01-1763* (2007).
2. Svoboda, J. and Cizek, V. "Pedestrian-vehicle collision: Vehicle design analysis", *SAE 2003-01-0896* (2003).
3. Svoboda, J., Solc, Z. and Cizek, V. "Analysis of collision between pedestrian and small car", *International Journal of Crashworthiness*, **8**(3), pp. 269-276 (2003).
4. Dunmore, M.C., Brooks, R., Madeley, N.J. and McNally, D.S. "The effect of leg fracture level and vehicle front-end geometry on pedestrian knee injury and response", *IMechE*, pp. 857-869 (2006).
5. Qiao, W. and Wang, X. "The simulation of vehicle-pedestrian collision and protection", *SAE 2007-01-3594* (2007).
6. Kendall, R., Meissner, R. and Crandall, J. "The causes of head Injury in vehicle-pedestrian impacts: Comparing the relative danger of vehicle and road surface", *SAE 2006-01-0462* (2006).
7. Pathare, R.V., Tawde, N. and Miraje, A. "Identification of key parameters for pedestrian impact safety", *SAE 2005-26-320* (2006).
8. Yao, J.F., Yang, J.K. and Fredriksson, R. "Reconstruction of head-to-hood impact in an automobile-to-child-pedestrian collision", *International Journal of Crashworthiness*, **11**(4), pp. 387-395 (2006).
9. Shahbeyk, S., Kamalan, A. and Osanlou, M. "A comparative study on vehicle aluminum and steel hood assemblies", *International Journal of Crashworthiness*, **8**(4), pp. 367-374 (2003).
10. Ikeda, K. and Ishitobi, H. "Development of aluminum hood structure for pedestrian protection", *SAE 2003-01-2793* (2003).
11. Schwarz, D., Bachem, H. and Opbroek, E. "Comparison of steel and aluminum hood with same design in view of pedestrian head impact", *SAE 2004-01-1605* (2004).
12. Kajzer, J., Matsui, Y., Ishikawa, H., Schroeder, G. and Bosch, U. "Shearing and bending effects at the knee joint at low speed lateral loading", *SAE 1999-01-0712* (1999).
13. Matsui, Y. "Effects of vehicle bumper height and impact velocity on type of lower extremity injury in vehicle-pedestrian accidents", *Accident Analysis and Prevention*, **37**(4), pp. 633-640 (2005).
14. Kuwahara, S., Hosokawa, T., Okada, K. and Mizuno, K. "Finite element analysis of pedestrian lower extremity injuries in car-to-pedestrian impacts", *SAE 2007-01-0755* (2007).
15. Hassel, E., Bosma, F., Vendrig, R. and Happee, R. "Method for leg protection of pedestrians and cyclists by vehicle front adaptation", *SAE 2007-26-009* (2006).
16. European Enhanced Vehicle-safety Committee (EEVC), *Improved Test Methods to Evaluate Pedestrian Protection Afforded by Passenger Cars*, EEVC Working Group 17 (1998).
17. Japan National Agency for Automotive Safety and Victim's Aid (www.nasva.go.jp).
18. Wordenweber, B. and Schafer, H. "Pedestrian protection", *SEA 2004-01-1282* (2004).
19. Matsui, Y., Wittek, A. and Konosu, A. "Comparison of pedestrian subsystem safety tests using impactors and full-scale dummy tests", *SAE 2002-01-1021* (2002).
20. Han, Y.H. and Lee, Y.W. "Optimization of bumper structure for pedestrian lower leg impact", *SAE 2002-01-0023* (2002).
21. Sapuan, S.M., Maleque, M.A., Hameedullah, M., Suddin, M.N. and Ismail, N. "A note on the conceptual design of polymeric composite automotive bumper system", *Journal of Materials Processing Technology*, **159**(2), pp. 145-151 (2005).

22. Davoodi, M.M., Sapuan, S.M. and Yunus, R. "Conceptual design of a polymer composite automotive bumper energy absorber", *Materials and Design*, **29**(7), pp. 1447-1452 (2008).

23. Shuler, S., Mooijman, F. and Nanda, A. "Bumper systems designed for both pedestrian protection and FMVSS requirements: Part design and testing", *SAE 2004-01-1610*.

24. *PAM-CRASH Solver Notes Manual*, ESI Group Software Product Co., Paris (2000).

25. Yu, H., Medri, M.B., Zhou, Q., DiMasi, F.P. and Bandak, F.A. "Head-neck finite element model of the crash test dummy THOR", *International Journal of Crashworthiness*, **9**(2), pp. 175-186 (2004).